

Meta-GGA exchange-correlation free energy density functional to increase the accuracy of warm dense matter simulations

Valentin V. Karasiev,* D. I. Mihaylov, and S. X. Hu
*Laboratory for Laser Energetics, University of Rochester,
250 East River Road, Rochester, New York 14623-1299, USA*

(Dated: 04 Feb 2022)

We discuss strategies for thermalization of the ground-state meta-generalized gradient approximation (meta-GGA) exchange-correlation (XC) functionals. A simple but accurate scheme is implemented via universal additive thermal correction to XC using a perturbative-like self-consistent approach. The additive correction with explicit temperature dependence is applied to the ground-state deorbitalized, strongly constrained and appropriately normed (SCAN-L) meta-GGA XC leading to thermal XC functional denoted here as T-SCAN-L. Thermal T-SCAN-L meta-GGA functional shows significant improvement in density functional theory calculation accuracy for warm dense matter by a factor of 3 to 10, achieving unprecedented accuracy of total pressure between a few tenths and $\sim 1\%$ when compared to traditional XC functionals, as demonstrated by the comparison to path-integral Monte Carlo simulations for helium equation of state. The T-SCAN-L calculations of dc conductivity of warm dense aluminum also give better agreement with experiments over other XC functionals such as PBE and SCAN-L.

PACS numbers:

Introduction. - High-energy density physics (HEDP) includes a complicated warm-dense matter (WDM) domain of state conditions which is characterized by elevated temperatures (from few to hundreds of eV) and pressures to 1 Mbar or greater. Accurate knowledge of equation of state, transport and optical properties describing possible phase transitions (eg. insulator-to-metal transition) across warm-dense regime plays an important role in planetary science, astrophysics and inertial confinement fusion¹⁻⁶. The two relevant expansion parameters, the Coulomb coupling parameter and the electron degeneracy parameter are of order unity in WDM regime. This is very distinct from the typical parameter space of plasma physics and ordinary condensed matter physics such that the classical plasma physics methods become inaccurate when extended into the WDM domain, and the standard condensed-matter physics methods might have poor transferability when extended well beyond near-ambient conditions. *Ab initio* molecular dynamics (AIMD)⁷⁻¹⁰ simulations based on the free-energy density functional theory (DFT)¹¹⁻¹³, in combination with the Kubo-Greenwood (KG) formulation for transport and optical properties^{14,15}, has proven to be a successful and key tool to understanding WDM and HED plasmas across different temperature regimes¹⁶⁻³².

DFT requires approximations for the exchange-correlation (XC) energy density functional, which effectively takes into account many-body interaction effects. It offers a self-consistent way to predict material properties with the possibility of systematic improvement of its accuracy through advancing XC functionals. Currently, the vast majority of DFT simulations of WDM and HED plasmas use the zero-temperature (ground-state) XC functionals without explicit temperature dependence, which were developed by the condensed-matter physics

and quantum chemistry communities, leading to neglect of thermal XC effects and degraded accuracy of predictions. The use of a ground-state XC functional is justified only at low electronic temperatures not exceeding a few tenths of the Fermi temperature or in the high-temperature limit when the XC contribution to the total free energy is negligible³³⁻³⁶. Recent development of the temperature-dependent Karasiev-Sjostrom-Dufty-Trickey (KSST)³⁷ local-density approximation (LDA) (see Ref.³⁸ for the corrected set of parameters corrKSST), the generalized gradient approximation (GGA)-type XC functional “KDT16”³⁸, and the thermal hybrid KDT0³⁹ have shown that thermal XC effects lower the dc electrical conductivity of low-density Al, yielding improved agreement with experiment³³, and can give up to a 20% difference in pressure³⁸ as compared to the zero-temperature Perdew-Burke-Ernzerhof (PBE)⁴⁰ calculations. Inclusion of thermal XC effects accounts for the softening of the deuterium Hugoniot at pressures above 300 GPa in agreement with recent experimental measurements^{41,42}. Thermal hybrid KDT0 provides a significant improvements for the electronic band gap at a wide range of temperatures as compared to the LDA and GGA rung functionals and to the ground-state PBE0 hybrid.

Inaccuracies of used XC functionals may affect not only the static properties related to equation of state; phase boundaries and DFT calculations of transport and optical properties of HED plasmas may suffer to a greater extent⁴³⁻⁴⁵, which elucidates the need for developing advanced XC functionals that can better describe the dissociation process and the band-gap closing dynamics. It must be noted that the temperature-dependent KDT16 GGA will not resolve these problems because it inherits the inaccuracy of PBE for the dissociation/melting and

band-gap predictions³⁹. Thermal hybrid KDT0 provides more realistic band gap predictions³⁹. However, electronic and optical properties in Kubo–Greenwood calculations to a large extent depend on ionic arrangement of snapshots generated along a particular MD trajectory. Therefore a fully consistent approach requires employment of the same XC functional in both the MD simulations and Kubo–Greenwood calculations making such simulations with hybrid functionals computationally impracticable³. For this reason, in present work all the comparisons are performed only between semi-local functionals, and performance of semi-local functionals with respect to hybrids at warm-dense conditions may need to be addressed in the future.

It would be not practical to develop a thermal XC functional applicable only at warm dense conditions. The approach taken by developers of the first *nonempirical* LDA, GGA, and hybrid XC free energy^{37–39} was to construct thermal functionals that at $T = 0$ K reduce to a known ground-state functional, such that the thermal XC functional is applicable across the entire range of temperatures without need to switch between XC functionals depending on state conditions. KDT16 GGA, for example, reduces to the ground-state PBE, such that KDT16 at low T inherits all advantages and drawbacks of its ground-state counterpart. The way to improve overall accuracy of the thermal GGA XC functional is to use the next rung approximation at zero T and construct thermally extended meta-GGA XC.

In this Letter we address this problem by developing a thermalization framework for XC functionals at the meta-GGA level of refinement and realization of a simple scheme via universal thermal XC additive correction at the GGA level of theory, which is applied to an accurate, at low T , ground-state meta-GGA XC. This thermal correction reduces to zero in the low- T limit; therefore, it could be used virtually with any ground-state XC functional without distorting its low- T performance.

Thermal correction is applied to the ground-state deorbitalized, strongly constrained, and appropriately normed semilocal density functional (SCAN-L)^{46–49}, to date one of the most-accurate meta-GGA XC functional, which, for example, is capable of accurately describing the liquid–liquid insulator-to-metal transition of warm dense hydrogen³. The resulting thermal meta-GGA XC functional, referred to here as T-SCAN-L, inherits the precision of the ground-state meta-GGA SCAN-L at low T , and most of the thermal XC effects are captured at the GGA level of theory, providing overall a much higher accuracy across the temperature regimes spanned by the WDM domain.

Construction of nonempirical thermal meta-GGA XC functionals.— Our strategy for thermalization of the ground-state functionals is based on extending of the constraints formulated in Ref.³⁸ to meta-GGA’s. Ta-

TABLE I: List of the ground-state and finite-temperature variables used in the GGA-level XC functionals. Ground state: ^aLDA exchange energy per particle; ^bLDA correlation energy per particle; ^creduced density gradient; ^ddimensionless density gradient defined in Ref.⁴⁰ as variable t .

$T = 0$ K	$T > 0$ K	Definition of $T > 0$ K variable
$\varepsilon_x^{\text{LDA}}(n)^a$	$f_x^{\text{LDA}}(n, T)$	Eq. (3) in Ref. ³⁸
$\varepsilon_c^{\text{LDA}}(n)^b$	$f_c^{\text{LDA}}(n, T)$	Eq. (21) in Ref. ³⁷
$s(n, \nabla n)^c$	$s_{2x}(n, \nabla n, T)$	Eq. (7) in Ref. ³⁸
$q(n, \nabla n)^d$	$q_c(n, \nabla n, T)$	Eq. (11) in Ref. ³⁸

ble I provides a list of ground-state variables and their finite-temperature counterparts used in the GGA framework. The temperature dependence of the XC gradients listed in Table I, as derived in Ref.³⁸, is consistent with the XC finite- T gradient expansion. Ground-state meta-GGA XC additionally depends on the noninteracting kinetic-energy-density variables. In the case of the deorbitalized SCAN-L functional, these variables are the Thomas–Fermi^{50,51}, von Weizsäcker⁵², and an orbital-free Laplacian-dependent kinetic-energy densities, used to define the chemical region detector $\alpha(n, \nabla n, \nabla^2 n)$ (see Ref.⁴⁸ for details). Proper T dependence of these kinetic-energy-related quantities is defined via kinetic and entropic GGA reduced density gradients $s_\tau(n, \nabla n, T)$ and $s_\sigma(n, \nabla n, T)$ derived in Ref.⁵³ and a set of T -dependent fourth order variables derived in Ref.⁵⁴ for the Laplacian-dependent orbital-free quantities. Such a *full* thermalization requires, however, a preliminary development of meta-GGA (Laplacian-dependent) noninteracting free energy framework and corresponding orbital-free noninteracting free-energy density functional (work currently in progress) to be used together with Thomas–Fermi and von Weizsäcker free-energy density terms to construct the T -dependent chemical energy detector $\alpha(n, \nabla n, \nabla^2 n, T)$. A simpler (not necessarily worse) GGA-level thermalization scheme includes only the usage of T -dependent variables listed in Table I instead of the ground-state ones in the ground-state SCAN-L functional $\varepsilon_x^{\text{LDA}}(n) \rightarrow f_x^{\text{LDA}}(n, T)$ and $s(n, \nabla n) \rightarrow s_{2x}(n, \nabla n, T)$ in the exchange; and $\varepsilon_c^{\text{LDA}}(n) \rightarrow f_c^{\text{LDA}}(n, T)$ and $q(n, \nabla n) \rightarrow q_c(n, \nabla n, T)$ in the correlation terms.

With increasing temperature, the electron density approaches the slowly-varying regime. This makes the finite-temperature second-order gradient expansion^{56–59} taking into account the leading corrections to the XC free-energy beyond the LDA. The KDT16 GGA functional, by construction, recovers the finite- T gradient expansion, therefore it is reasonable to expect that the leading contributions to thermal XC effects are taken into account by the T -dependent LDA and GGA XC terms. Thereby thermal XC corrections beyond the GGA level are expected to be small; therefore in the following

we propose a simple perturbative-like self-consistent approach via a universal thermal additive correction treated self-consistently, similar to the idea used in Ref.⁵⁵ to construct GGA XC with additive thermal LDA correction. The KDT16 XC free energy in the zero- T limit reduces to the ground-state PBE by construction

$$\lim_{T \rightarrow 0} \mathcal{F}_{xc}^{\text{KDT16}}[n, T] \approx E_{xc}^{\text{PBE}}[n], \quad (1)$$

a choice driven by popularity of the PBE functional, and by availability of pseudo-potentials and projector augmented wave (PAW) data sets generated by using the PBE XC. Given the quality of SCAN-L functional at zero temperature, we propose a simple temperature-dependent meta-GGA

$$\mathcal{F}_{xc}^{\text{meta-GGA}}[n, T] = E_{xc}^{\text{meta-GGA}}[n] + \Delta \mathcal{F}_{xc}^{\text{GGA}}[n, T], \quad (2)$$

with the additive thermal correction defined as follows:

$$\Delta \mathcal{F}_{xc}^{\text{GGA}}[n, T] := \mathcal{F}_{xc}^{\text{KDT16}}[n, T] - E_{xc}^{\text{PBE}}[n] \quad (3)$$

and meta-GGA=SCAN-L. Definition Eqs. (2) and (3) can also be rearranged to the form of thermal GGA plus a zero-temperature meta-GGA correction

$$\mathcal{F}_{xc}^{\text{meta-GGA}}[n, T] = \mathcal{F}_{xc}^{\text{KDT16}}[n, T] + \Delta E_{xc}^{\text{meta-GGA}}[n], \quad (4)$$

where the $\Delta E_{xc}^{\text{meta-GGA}}[n] := E_{xc}^{\text{meta-GGA}}[n] - E_{xc}^{\text{PBE}}[n]$ term accounts for the zero-temperature meta-GGA corrections above the GGA level of theory. Explicit functional form defined by Eqs. (2), (3) is used in standard fully self-consistent DFT calculations with local XC potential calculated as a functional derivative of $\mathcal{F}_{xc}^{\text{meta-GGA}}[n, T]$ with respect to electron density n . Each term in the above equations is evaluated at self-consistent minimizing density corresponding to given thermodynamic conditions of material density and temperature. The full set of equations for each term in Eqs. (2)-(3) including definitions of the finite- T LDA XC is given in the Supplemental Material⁶⁰ (see also Refs.⁶¹⁻⁶³).

It follows from Eq. (1) that in the zero- T limit, the thermal additive correction [Eq. (3)] reduces to zero, $\lim_{T \rightarrow 0} \Delta \mathcal{F}_{xc}^{\text{GGA}}[n, T] \approx 0$; therefore the thermal meta-GGA reduces to their zero-temperature counterpart

$$\lim_{T \rightarrow 0} \mathcal{F}_{xc}^{\text{meta-GGA}}[n, T] \approx E_{xc}^{\text{meta-GGA}}[n], \quad (5)$$

preserving the meta-GGA accuracy at low T . In the high- T limit, the minimizing electron density becomes slowly varying and approaches the homogeneous electron gas limit. Reduced density gradients and reduced Laplacian employed in construction of the ground-state GGA and meta-GGA vanish. The ground-state PBE GGA and SCAN-L meta-GGA by construction reduce

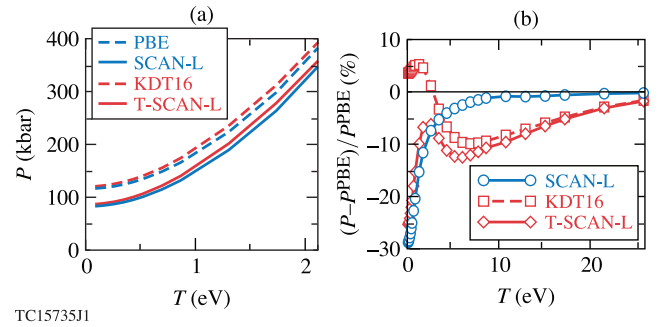


FIG. 1: (a) Electronic pressure as a function of temperature for sc-H at $\rho = 0.60 \text{ g/cm}^3$ calculated with the PBE and KDT16 GGA, and with the SCAN-L and T-SCAN-L meta-GGA XC functionals. (b) Corresponding relative difference with respect to the PBE values, $(P - P^{\text{PBE}})/P^{\text{PBE}}$, as a function of electronic temperature.

to the ground-state LDA XC in the homogeneous density limit. In this way the ground-state GGA and meta-GGA functionals, if evaluated at implicitly T -dependent minimizing density, approach the temperature-independent LDA limit, $\lim_{T \rightarrow \infty} E_{xc}^{\text{meta-GGA}}[n] \approx E_{xc}^{\text{LDA}}[n]$ and $\lim_{T \rightarrow \infty} E_{xc}^{\text{PBE}}[n] \approx E_{xc}^{\text{LDA}}[n]$ (i.e., $E_{xc}^{\text{meta-GGA}}[n] \approx E_{xc}^{\text{PBE}}[n]$ at high T). Therefore, at high temperatures, the thermal meta-GGA Eq. (4), evaluated at the minimizing density, reduces to the KDT16 (which in turn, by construction, reduces to the finite- T LDA):

$$\mathcal{F}_{xc}^{\text{meta-GGA}}[n, T] \Big|_{T \gg 1} \approx \mathcal{F}_{xc}^{\text{KDT16}}[n, T] \approx \mathcal{F}_{xc}^{\text{LDA}}[n, T]. \quad (6)$$

Other constraints and exact conditions satisfied by the T-SCAN-L XC are listed in Sec. IV of Supplemental Material.

Thermal meta-GGA Eq. (2) accounts for thermal XC correction via temperature-dependent LDA and reduced density-gradient terms used in the construction of the KDT16 at the GGA level of theory. Reduced-density Laplacian and orbital-free kinetic energy density used in deorbitalized SCAN-L remain without explicit temperature dependence. Use of T -dependent reduced Laplacian may account for additional fourth order thermal XC effects that, in general, are expected to be small.

Demonstrative WDM applications.- To investigate the performance of the new T-SCAN-L meta-GGA functional with respect to the existing PBE, SCAN-L, and KDT16 approximations and to estimate XC ground-state meta-GGA inhomogeneity effects (defined as the difference between the SCAN-L and PBE pressures), thermal XC effects at the GGA level (difference between the KDT16 and PBE), and combined XC thermal and inhomogeneity effects at the meta-GGA level (difference between the T-SCAN-L and PBE pressures), we performed a set of static and AIMD simulations using these four XC functionals.

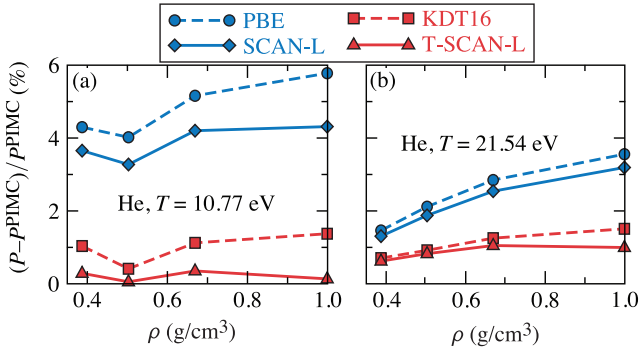
Figure 1(a) shows electronic pressure as a function of temperature for a model system of hydrogen in simple cubic lattice (sc-H) at 0.60 g/cm^3 . At low T , in agreement with Eqs. (1) and (5), pressure from calculations with thermal KDT16 and T-SCAN-L XC functionals (dashed and solid red curves, respectively) is identical to results obtained with ground-state PBE and SCAN-L functionals (dashed and solid blue curves, respectively). Thermal functional pressures (red curves) start to deviate from their ground-state counterparts as temperature increases.

The relative magnitude of XC ground-state meta-GGA inhomogeneity effects referenced to the PBE ground-state GGA values $[(P^{\text{SCANL}} - P^{\text{PBE}})/P^{\text{PBE}}]$, XC thermal effects at the GGA level $[(P^{\text{KDT16}} - P^{\text{PBE}})/P^{\text{PBE}}]$, and XC thermal and inhomogeneity effects at the meta-GGA level $[(P^{\text{TSCANL}} - P^{\text{PBE}})/P^{\text{PBE}}]$ are shown in Fig. 1(b). The relative difference between the ground-state SCAN-L and PBE pressures reaches the large value of $\approx 30\%$ at low T and decays below 5% at temperatures above 5 eV , meaning that the zero- T meta-GGA correction $\Delta E_{\text{xc}}^{\text{meta-GGA}}$ defined in the in-line equation below Eq. (4) vanishes at high T (the discussion below Eq. (5) explains the reason). Thermal XC effects at the GGA level (KDT16, dashed red curve) reach the maximum magnitude ($\sim 10\%$) at T near 6.5 eV (reduced temperature t is about 0.4) and remain at the level above 5% up to 20 eV ($t \approx 1$). As expected, the thermal T-SCAN-L meta-GGA preserves the accuracy of the ground-state SCAN-L at low T (the accurate description of hydrogen in this dense regime by the the ground-state SCAN-L XC at low T , when XC thermal effects are negligible, was recently demonstrated in Ref.³) and converges to the thermal KDT16 at high T , providing a smooth interpolation at intermediate temperatures. Figure 1(b) clearly demonstrates that the sum of the SCAN-L (solid blue) and KDT16 (dashed red) curves agrees very well with the T-SCAN-L (solid red) one, meaning that the combined XC thermal and inhomogeneity meta-GGA effects correspond to the sum $\Delta \mathcal{F}_{\text{xc}}^{\text{GGA}} + \Delta E_{\text{xc}}^{\text{meta-GGA}}$ as expected. Given that the T-SCAN-L smoothly interpolates between the ground-state meta-GGA and finite- T KDT16, we expect that the T-SCAN-L results are most accurate across the entire temperature range. (Remark: at very high temperatures the differences between calculations with thermal and ground-state XC functionals vanish due to the fact that XC contribution to the total free energy becomes negligible compared to the dominating non-interacting free-energy term³⁸.) Very recently the T-SCAN-L XC in combination with the long-range van der Waals rVV10 functional⁶⁴ was used to establish a first-principle equation of state table of deuterium and demonstrated an improvement of accuracy as compared to the treatment with the ground-state PBE treatment.

AIMD simulations that demonstrate the superior accuracy of the new T-SCAN-L meta-GGA functional are for

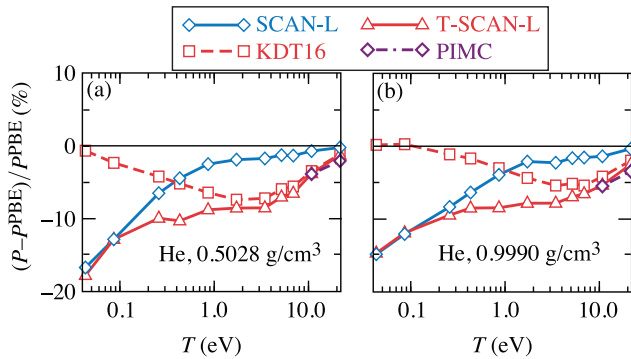
dense helium. Figure 2 compares relative errors for total pressures obtained from DFT simulations with four XC functionals and high-quality path-integral Monte Carlo (PIMC) reference data⁶⁵ for $T = 10.77 \text{ eV}$ and 21.54 eV (PIMC data are not available for T below 10.77 eV , and Kohn-Sham DFT simulations for this range of material densities and temperatures above 21.54 eV are too expensive computationally). PIMC is an efficient *first-principles* simulation technique for quantum systems at finite temperature that accurately takes into account the Coulomb interaction between electrons using pair-density matrices and therefore can be used to benchmark approximate XC density functionals at elevated temperature³³. Both ground-state functionals (PBE and SCAN-L) systematically overestimate the total pressure: the relative error with respect to the reference PIMC data is between 4.2% and 5.8% at $T = 10.77 \text{ eV}$. In contrast, the T-SCAN-L total pressures are in excellent agreement with the PIMC values, demonstrating unprecedented accuracy between 0.05% and 0.35% for this range of densities. Relative differences between the KDT16 and PIMC values are larger as compared to the T-SCAN-L values and range from 0.4% to 1.4% . These comparisons show that T-SCAN-L calculations can improve the DFT simulation accuracy for He at these warm dense conditions by a factor of ~ 3 to 10 over the widely used XC functionals (PBE, SCANL, and KDT16). This clearly demonstrates that the T-SCAN-L meta-GGA functional can accurately capture combined XC thermal and nonhomogeneity effects. When temperature increases to 21.54 eV , the relative error of the ground-state functionals reduces to the range between 1.3% and 3.6% (because the XC contribution becomes less important as compared to the noninteracting free-energy term at high T), while the relative difference between T-SCAN-L and PIMC values is still less than $\sim 1\%$. Kohn-Sham calculations for this system at temperatures much higher than 20 eV are not feasible. However, in accordance with discussion of high- T results shown in Fig. 1(b), we expect that eventually, with increase of temperature, all calculations with the thermal and ground state functionals will converge to the same values, making the PBE XC an accurate reference in the high- T limit.

Figure 3 shows the relative differences between the SCAN-L, KDT16, T-SCAN-L, and PBE pressures as a function of temperature at two different densities: $\rho_{\text{He}} = 0.5028 \text{ g/cm}^3$ and 0.9990 g/cm^3 . The overall picture is similar to that observed in Fig. 1 for the model system: at low T , thermal KDT16 and T-SCAN-L reduce to their ground-state counterparts, PBE and SCAN-L, respectively. The zero- T meta-GGA correction $\Delta E_{\text{xc}}^{\text{meta-GGA}}$ becomes small at $T > 1 \text{ eV}$; XC thermal effects, as described by the KDT16 GGA XC, grow to values almost 10% at T near few eV and start to decrease at T above 10 eV . The new T-SCAN-L smoothly interpolates between



TC15736J1

FIG. 2: The relative error of total pressure from AIMD simulations of warm dense He using PBE, SCAL-L, KDT16, and T-SCAN-L XC functionals calculated with respect to the reference PIMC results and shown as a function of material density for two temperatures.

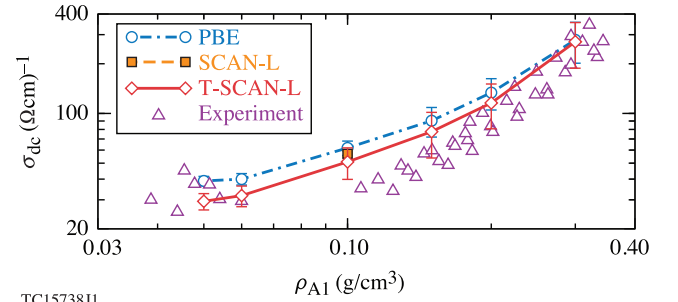


TC15737J1

FIG. 3: Relative difference between the total pressure from the DFT calculations with SCAN-L, KDT16, T-SCAN-L, and PBE XC. The PIMC relative pressure difference with respect to the same PBE XC values is shown for comparison.

the ground-state SCAN-L, preserving its accuracy at low T , and the thermal KDT16 at high temperature, providing a description of combined XC thermal and nonhomogeneity effects at the entire temperature range. These combined effects remain at relatively large values above 5% for temperatures up to ≈ 10 eV and slowly drop for higher T .

Finally, we examine how T-SCAN-L may affect the DFT prediction of transport properties of warm dense matters. Results of simulations that probe the accuracy of thermal T-SCAN-L functional for electrical conductivity of warm dense Al are shown in Fig. 4. The direct current (dc) conductivity from AIMD and Kubo-Greenwood^{14,15} calculations with the ground-state PBE and thermal T-SCAN-L functionals is compared to the experimental data⁶⁶ at $T = 10$ kK in the density range between 0.05 and 0.30 g/cm³. Ground-state PBE overestimates conductivity for densities ≤ 0.20 g/cm³. Previously it was shown that the explicitly T -dependent KSDT functional lowers the dc conductivity³³ as compared to



TC15738J1

FIG. 4: Aluminum dc conductivity as a function of density from calculations with T -dependent T-SCAN-L, and ground-state PBE and SCAN-L (at $\rho = 0.10$ g/cm³ only) XC functionals along the $T = 10$ -kK isotherm. The standard deviations shown as error bars correspond to averaging over the snapshots.

the ground-state LDA. Thermal T-SCAN-L behaves similarly, by lowering the dc conductivity (as compared to the ground-state PBE) toward the experimental data. At $\rho_{\text{Al}} = 0.30$ g/cm³, results from both functionals converge and agree with experiment. SCAN-L dc conductivity, calculated for one density only, 0.10 g/cm³, is roughly in between the PBE and T-SCAN-L values, demonstrating that combined thermal and nonhomogeneity XC effects contribute to transport properties.

Summary.- The *full* thermalization framework and a simpler one using thermal LDA- and GGA-level variables to construct thermally extended meta-GGA XC functionals have been discussed. The *fully* thermalized scheme involves thermalization of the kinetic energy related terms and requires a preliminary development of non-interacting free energy density functionals at the meta-GGA level of refinement. These functionals, besides the standard constraints related to the zero- T and high- T limits and the scaling related constraints discussed in⁵³ should recover the 4th order slow-varying density gradient expansion for the noninteracting free energy⁶⁹⁻⁷¹ to guarantee the correct treatment of the Laplacian-dependent (4th-order) terms in meta-GGA XC functional. However, a reasonable expectation is that the *full* thermalization will provide only a minor correction to predicted properties in WDM regime.

The simplest scheme, which uses a universal additive thermal correction and a perturbative-like self-consistent approach, has been implemented, leading to thermal T-SCAN-L functional. The nonempirical T-SCAN-L meta-GGA density functional takes into account combined thermal and nonhomogeneity effects at the meta-GGA level providing a significantly higher accuracy for DFT to better predict material properties in the WDM regime, as compared to the thermal KDT16, and to the ground-state PBE and SCAN-L XC functionals. In the zero-temperature limit, T-SCAN-L reduces to its ground-state counterpart, therefore preserving the SCAN-L meta-

GGA level of accuracy at low T . Virtually any ground-state meta-GGA XC functional can be thermally extended into an XC free-energy functional via our proposed scheme. The thermalization scheme carries over directly to the regularized-restored r^2 SCAN-L^{67,68}, which mostly eliminates numerical instabilities and related convergence issues of SCAN-L, to yield thermal T- r^2 SCAN-L [Eq. (4) with meta-GGA= r^2 SCAN-L]. Although T- r^2 SCAN-L has not yet been tested and all results of present work have been obtained with T-SCAN-L, we expect that T- r^2 SCAN-L will provide a virtually identical level of accuracy as T-SCAN-L.

Acknowledgments.- This report was prepared as an account of work sponsored by an agency of the U.S. Government. Neither the U.S. Government nor any agency thereof, nor any of their employees, makes any warranty, express or implied, or assumes any legal liability or responsibility for the accuracy, completeness, or usefulness of any information, apparatus, product, or process dis-

closed, or represents that its use would not infringe privately owned rights. Reference herein to any specific commercial product, process, or service by trade name, trademark, manufacturer, or otherwise does not necessarily constitute or imply its endorsement, recommendation, or favoring by the U.S. Government or any agency thereof. The views and opinions of authors expressed herein do not necessarily state or reflect those of the U.S. Government or any agency thereof.

This material is based upon work supported by the Department of Energy National Nuclear Security Administration under Award Number DE-NA0003856 and US National Science Foundation PHY Grant No. 1802964. This research used resources of the National Energy Research Scientific Computing Center, a DOE Office of Science User Facility supported by the Office of Science of the U.S. Department of Energy under Contract No. DE-AC02-05CH11231.

* Corresponding Author: vkarsev@lle.rochester.edu

- ¹ J.J. Fortney and N. Nettelmann, “The Interior Structure, Composition, and Evolution of Giant Planets”, *Space Sci. Rev.* **152**, 423-447 (2010).
- ² W. Lorenzen, B. Holst, and R. Redmer, “Metallization in hydrogen-helium mixtures”, *Phys. Rev. B* **84**, 235109 (2011).
- ³ J. Hinz, V.V. Karasiev, S.X. Hu, M. Zaghoo, D. Mejía-Rodríguez, S.B. Trickey, and L. Calderín, “Fully consistent density functional theory determination of the insulator-metal transition boundary in warm dense hydrogen” *Phys. Rev. Res.* **2**, 032065(R) (2020).
- ⁴ C.A. Iglesias, F.J. Rogers, and D. Saumon, “Density effects on the opacity of cool helium white dwarf”, *Astrophys. J. Lett.* **569**, L111 (2002).
- ⁵ S.X. Hu, V.N. Goncharov, T.R. Boehly, R.L. McCrory, S. Skupsky, L.A. Collins, J.D. Kress, and B. Militzer, Impact of first-principles properties of deuterium-tritium on inertial confinement fusion target designs, *Phys. Plasmas* **22**, 056304 (2015).
- ⁶ V.V. Karasiev, S.X. Hu, “Unraveling the intrinsic atomic physics behind x-ray absorption line shifts in warm dense silicon plasmas”, *Phys. Rev. E* **103**, 033202 (2021).
- ⁷ R.N. Barnett and U. Landman, “Born-Oppenheimer Molecular-Dynamics Simulations of Finite Systems: Structure and Dynamics of (H₂O)₂”, *Phys. Rev. B* **48** (4), 2081-2097 (1993).
- ⁸ D. Marx and J. Hutter, “Ab Initio Molecular Dynamics: Theory and Implementation”, in *Modern Methods and Algorithms of Quantum Chemistry*, J. Grotendorst ed., John von Neumann Institute for Computing, (Jülich, NIC Series, Vol. 1, 2000) 301-478 and references therein.
- ⁹ J.S. Tse, “Ab Initio Molecular Dynamics with Density Functional Theory”, *Ann. Rev. Phys. Chem.* **53** (1), 249-290 (2002).
- ¹⁰ *Ab Initio Molecular Dynamics: Basic Theory and Advanced Methods*, D. Marx and J. Hutter, (Cambridge University Press, Cambridge, 2009) and references therein.
- ¹¹ N.D. Mermin, “Thermal Properties of the Inhomogeneous Electron Gas”, *Phys. Rev.* **137** (5A), A1441-A1443 (1965).
- ¹² W. Kohn and L.J. Sham, “Self-Consistent Equations Including Exchange and Correlation Effects”, *Phys. Rev.* **140** (5A), A1133-A1138 (1965).
- ¹³ M.V. Stoitsov and I.Zh. Petkov, “Density Functional Theory at Finite Temperatures”, *Annals Phys.* **184**, 121-147 (1988).
- ¹⁴ R. Kubo, “Statistical-Mechanical Theory of Irreversible Processes. I. General Theory and Simple Applications to Magnetic and Conduction Problems”, *J. Phys. Soc. Jpn.* **12** (6), 570-586 (1957).
- ¹⁵ D. A. Greenwood, “The Boltzmann Equation in the Theory of Electrical Conduction in Metals”, *Proc. Phys. Soc.* **71**, 585-596 (1958).
- ¹⁶ *Frontiers and Challenges in Warm Dense Matter*, F. Graziani, M.P. Desjarlais, R. Redmer, and S.B. Trickey eds. (Springer Verlag, Heidelberg, 2014)
- ¹⁷ S.X. Hu, “Continuum Lowering and Fermi-Surface Rising in Strongly Coupled and Degenerate Plasmas”, *Phys. Rev. Lett.* **119** (6), 065001(1-6) (2017).
- ¹⁸ B.B.L. Witte, L.B. Fletcher, E. Galtier, E. Gamboa, H.J. Lee, U. Zastrau, R. Redmer, S.H. Glenzer, and P. Sperling, Warm Dense Matter Demonstrating Non-Drude Conductivity from Observations of Nonlinear Plasmon Damping, *Phys. Rev. Lett.* **118**, 225001(1-6) (2017).
- ¹⁹ M.D. Knudson, M.P. Desjarlais, A. Becker, R.W. Lemke, K.R. Cochrane, M.E. Savage, D.E. Bliss, T.R. Mattsson, R. Redmer, Direct Observation of an Abrupt Insulator-to-Metal Transition in Dense Liquid Deuterium, *Science*, **348**, 1455-1460 (2015).
- ²⁰ S.M. Vinko, O. Ciricosta, and J.S. Wark, “Density Functional Theory Calculations of Continuum Lowering in Strongly Coupled Plasmas”, *Nat. Commun.* **5**, 3533(1-7)

- (2014); DOI: 10.1038/ncomms4533
- 21 S.X. Hu, L.A. Collins, J.P. Colgan, V.N. Goncharov, and D.P. Kilcrease, “Optical Properties of Highly Compressed Polystyrene: An *ab initio* Study”, *Phys. Rev. B* **96**, 144203(1-11) (2017).
 - 22 Y.H. Ding, and S.X. Hu, “First-Principles Equation-of-State Table of Beryllium Based on Density-Functional Theory Calculations”, *Phys. Plasmas* **24**, 062702(1-10) (2017).
 - 23 S.X. Hu, R. Gao, Y. Ding, L.A. Collins, and J.D. Kress, “First-Principles Equation-of-State Table of Silicon and its Effects on High-Energy-Density Plasma Simulations”, *Phys. Rev. E* **95**, 043210(1-8) (2017).
 - 24 S.X. Hu, L.A. Collins, V.N. Goncharov, J.D. Kress, R.L. McCrory, and S. Skupsky, “First-Principles Equation of State of Polystyrene and its Effect on Inertial Confinement Fusion Implosions”, *Phys. Rev. E* **92**, 043104(1-7) (2015).
 - 25 F. Dorchies, F. Festa, V. Recoules, O. Peyrusse, A. Benuzzi-Mounaix, E. Brambrink, A. Levy, A. Ravasio, M. Koenig, T. Hall, and S. Mazevet, “X-ray Absorption *K* Edge as a Diagnostic of the Electronic Temperature in Warm Dense Aluminum”, *Phys. Rev. B* **92**, 085117(1-5) (2015).
 - 26 S.X. Hu, L.A. Collins, T.R. Boehly, J.D. Kress, V.N. Goncharov, and S. Skupsky, “First-principles Thermal Conductivity of Warm-Dense Deuterium Plasmas for Inertial Confinement Fusion Applications”, *Phys. Rev. E* **89**, 043105(1-10) (2014).
 - 27 T. Sjostrom, S. Crockett, and S. Rudin, “Multiphase Aluminum Equations of State via Density Functional Theory”, *Phys. Rev. B* **94**, 144101(1-10) (2016).
 - 28 F. Dorchies and V. Recoules, “Non-Equilibrium Solid-to-Plasma Transition Dynamics Using XANES Diagnostic”, *Physics Reports* **657**, 1-26 (2016).
 - 29 N. Jourdain, L. Lecherbourg, V. Recoules, P. Renaudin, and F. Dorchies, “Electron-Ion Thermal Equilibration Dynamics in Femtosecond Heated Warm Dense Copper”, *Phys. Rev. B* **97**, 075148(1-8) (2018).
 - 30 T. Sjostrom, and J. Daligault, “Nonlocal orbital-free non-interacting free-energy functional for warm dense matter”, *Phys. Rev. B* **88**, 195103(1-6) (2018).
 - 31 T. Sjostrom, and J. Daligault, “Fast and Accurate Quantum Molecular Dynamics of Dense Plasmas Across Temperature Regimes”, *Phys. Rev. Lett.* **113**, 155006(1-5) (2014).
 - 32 M.W.C. Dharma-wardana, “Ionization of carbon at 10–100 times the diamond density and in the 10⁶ K temperature range”, *Phys. Rev. E* **104**, 015201(1-9) (2021).
 - 33 V.V. Karasiev, L. Calderín, and S.B. Trickey, *Phys. Rev. E* **93**, 063207 (2016).
 - 34 V.V. Karasiev, S.B. Trickey, and J.W. Dufty, *Phys. Rev. B* **99**, 195134 (2019).
 - 35 K. Ramakrishna, T. Dornheim, and J. Vorberger, “Influence of finite temperature exchange-correlation effects in hydrogen”, *Phys. Rev. B* **101**, 195129 (2020).
 - 36 M. Bonitz, T. Dornheim, Zh.A. Moldabekov, S. Zhang, P. Hamann, H. Kählert, A. Filinov, K. Ramakrishna, and J. Vorberger, “Ab initio simulation of warm dense matter”, *Phys. Plasmas* **27**, 042710(1-24) (2020).
 - 37 V.V. Karasiev, T. Sjostrom, J. Dufty, and S.B. Trickey, “Accurate Homogeneous Electron Gas Exchange-Correlation Free Energy for Local Spin-Density Calculations”, *Phys. Rev. Lett.* **112** (7), 076403(1-5) (2014).
 - 38 V.V. Karasiev, J. Dufty, and S.B. Trickey, “Non-empirical Semi-local Free-Energy Density Functional for Matter Under Extreme Conditions”, *Phys. Rev. Lett.* **120**, 076401(1-7) (2018).
 - 39 D.I. Mihaylov, V.V. Karasiev, and S.X. Hu, “Thermal hybrid exchange-correlation density functional for improving the description of warm dense matter”, *Phys. Rev. B* **101**, 245141(1-6) (2020).
 - 40 J.P. Perdew, K. Burke, and M. Ernzerhof, “Generalized Gradient Approximation Made Simple”, *Phys. Rev. Lett.* **77**, 3865-3868 (1996) and the references therein; erratum *ibid.* **78**, 1396 (1997).
 - 41 V.V. Karasiev, S.X. Hu, M. Zaghoo, and T.R. Boehly, “Exchange-correlation thermal effects in shocked deuterium: Softening the principal Hugoniot and thermophysical properties”, *Phys. Rev. B* **99**, 214110 (2019).
 - 42 A. Fernandez-Pañella, M. Millot, D. E. Fratanduono, M. P. Desjarlais, S. Hamel, M. C. Marshall, D. J. Erskine, P. A. Sterne, S. Haan, T. R. Boehly, G. W. Collins, J. H. Eggert, and P. M. Celliers, *Phys. Rev. Lett.* **122**, 255702 (2019).
 - 43 M.A. Barrios, D.G. Hicks, T.R. Boehly, D.E. Fratanduono, J.H. Eggert, P.W. Celliers, G.W. Collins, and D.D. Meyerhofer, “High-Precision Measurements of the Equation of State of Hydrocarbons at 1–10 Mbar using Laser-driven Shock Waves”, *Phys. Plasmas* **17**, 056307(1-14) (2010).
 - 44 G. Huser, V. Recoules, N. Ozaki, T. Sano, Y. Sakawa, G. Salin, B. Albertazzi, K. Miyaniishi, and R. Kodama, “Experimental *Ab Initio* Investigations of Microscopic Properties of Laser-Shocked Ge-doped Ablator”, *Phys. Rev. E* **92**, 063108(1-14) (2015).
 - 45 S.X. Hu, L.A. Collins, T.R. Boehly, Y.H. Ding, P.B. Radha, V.N. Goncharov, V.V. Karasiev, G.W. Collins, S.P. Regan, and E.M. Campbell, “A Review on ab initio Studies of Static, Transport, and Optical Properties of Polystyrene under Extreme Conditions for Inertial Confinement Fusion Applications”, *Phys. Plasmas* **25**, 056306(1-15) (2018).
 - 46 J. Sun, A. Ruzsinszky, and J.P. Perdew, “Strongly Constrained and Appropriately Normed Semilocal Density Functional”, *Phys. Rev. Lett.* **115**, 036402(1-6) (2015).
 - 47 H. Peng, Z.H. Yang, J.P. Perdew, and J. Sun, “Versatile van der Waals Density Functional Based on a Meta-Generalized Gradient Approximation”, *Phys. Rev. X* **6**, 041005(1-15) (2016).
 - 48 D. Mejia-Rodriguez, and S.B. Trickey, “Deorbitalization Strategies for Meta-Generalized-Gradient-Approximation Exchange-Correlation Functionals” *Phys. Rev. A* **96**, 052512(1-10) (2017).
 - 49 D. Mejia-Rodriguez, and S.B. Trickey, “Deorbitalized Meta-GGA Exchange-Correlation Functionals in Solids” *Phys. Rev. B* **98**, 115161(1-9) (2018).
 - 50 L.H. Thomas, “The Calculation of Atomic Fields”, *Proc. Camb. Phil. Soc.* **23**, 542-548 (1927).
 - 51 E. Fermi, “Un Metodo Statistico per la Determinazione di alcune Proprietà dell’Atomo”, *Rend. Accad. Nazl. Lincei* **6**, 602-607 (1927).
 - 52 C.F. von Weizsäcker, “Zur Theorie de Kernmassen”, *Z. Phys.* **96**, 431-458 (1935).
 - 53 V.V. Karasiev, T. Sjostrom, and S.B. Trickey,

- “Generalized-Gradient-Approximation Noninteracting Free-Energy Functionals for Orbital-Free Density Functional Calculations”, *Phys. Rev. B* **86**, 115101(1-11) (2012).
- ⁵⁴ V.V. Karasiev, D. Chakraborty, and S.B. Trickey, “Improved Analytical Representation of Combinations of Fermi-Dirac Integrals for Finite-temperature Density Functional Calculations”, *Comput. Phys. Commun.* **192**, 114-123 (2015).
- ⁵⁵ T. Sjöström and J. Daligault, “Gradient corrections to the exchange-correlation free energy”, *Phys. Rev. B* **90**, 155109(1-6) (2014).
- ⁵⁶ E. Dunlap and D.J.W. Geldart, *Can. J. Phys.* **72**, 1 (1994).
- ⁵⁷ M.L. Glasser, D.J.W. Geldart, and E. Dunlap, *Can. J. Phys.* **72**, 7 (1994).
- ⁵⁸ E. Dunlap, and D.J.W. Geldart, *Can. J. Phys.* **72**, 14 (1994).
- ⁵⁹ D.J.W. Geldart, *Top. Curr. Chem.* **180**, 31 (1996).
- ⁶⁰ See Supplemental Material.
- ⁶¹ J.W. Dufty and S.B. Trickey, *Mol. Phys.* **114**, 988 (2016).
- ⁶² J.P. Perdew, and Y. Wang, *Phys. Rev. B* **45**, 13244 (1992).
- ⁶³ S. Pittalis, C.R. Proetto, A. Floris, A. Sanna, C. Bersier, K. Burke, and E.K.U. Gross, *Phys. Rev. Lett.* **107**, 163001 (2011).
- ⁶⁴ O.A. Vydrov and T. Van Voorhis, “Nonlocal Van Der Waals Density Functional Made Simple”, *Phys. Rev. Lett.* **103**, 063004(1-4) (2009).
- ⁶⁵ B. Militzer, “Path integral Monte Carlo and density functional molecular dynamics simulations of hot, dense helium”, *Phys. Rev. B* **79**, 155105(1-18) (2009).
- ⁶⁶ A.W. DeSilva, and J.D. Katsouros, “Electrical conductivity of dense copper and aluminum plasmas”, *Phys. Rev. E* **57**, 5945 (1998).
- ⁶⁷ J.W. Furness, A.D. Kaplan, J. Ning, J.P. Perdew, and J. Sun, *J. Phys. Chem. Lett.* **11**, 8208 (2020).
- ⁶⁸ . D. Mejia-Rodriguez, and S.B. Trickey, *Phys. Rev. B* **102**, 121109(R)(1-4) (2020).
- ⁶⁹ D.J.W. Geldart, and E. Sommer, *Phys. Lett.* **108A**, 103 (1985).
- ⁷⁰ D.J.W. Geldart, and E. Sommer, *Phys. Rev. B* **32**, 7694 (1985).
- ⁷¹ J. Bartel, M. Brack, and M. Durand, *Nucl. Phys. A* **445**, 263 (1985).

Supplemental Material -

“ Meta-GGA exchange-correlation free energy density functional to increase the accuracy of warm dense matter simulations ”

Valentin V. Karasiev,* D. I. Mihaylov, and S. X. Hu
*Laboratory for Laser Energetics, University of Rochester,
 250 East River Road, Rochester, New York 14623-1299, USA*

I. PBE EXCHANGE AND CORRELATION

The PBE ground-state spin-unpolarized exchange-correlation energy density functional is a sum of exchange and correlation

$$E_{xc}^{\text{PBE}}[n] = E_x^{\text{PBE}}[n] + E_c^{\text{PBE}}[n], \quad (\text{S1})$$

where exchange functional is given in terms of local density approximation (LDA) exchange energy per particle, $\varepsilon_x^{\text{LDA}}$, and the generalized gradient approximation (GGA) enhancement factor¹

$$E_x^{\text{PBE}}[n] = \int n(\mathbf{r}) \varepsilon_x^{\text{LDA}}(n) F_x^{\text{PBE}}(s) d\mathbf{r}, \quad (\text{S2})$$

$$\varepsilon_x^{\text{LDA}}(n) = -\frac{3}{4} \left(\frac{3}{\pi} \right)^{1/3} n^{1/3}, \quad (\text{S3})$$

$$F_x^{\text{PBE}}(s) = 1 + \kappa - \frac{\kappa}{1 + \frac{\mu s^2}{\kappa}}, \quad (\text{S4})$$

with $\kappa = 0.804$ and $\mu = 0.21951$, which is a function of ground-state (temperature independent) reduced density gradient,

$$s(n, \nabla n) = \frac{|\nabla n|}{2(3\pi^2)^{1/3} n^{4/3}}. \quad (\text{S5})$$

The correlation energy density functional is

$$E_c^{\text{PBE}}[n] = \int n(\mathbf{r}) \varepsilon_c^{\text{PBE}}(n, \nabla n) d\mathbf{r}, \quad (\text{S6})$$

where the PBE ground-state correlation energy per particle in notations of Ref.² is given by a function of density and density gradient

$$\varepsilon_c^{\text{PBE}}(n, \nabla n) = \varepsilon_c^{\text{LDA}}(n) + H(\varepsilon_c^{\text{LDA}}, \zeta = 0, q), \quad (\text{S7})$$

$\varepsilon_c^{\text{LDA}}[n]$ is the LDA correlation energy per particle (PBE uses the Perdew-Wang parametrization³), ζ is the spin-polarization fraction, and q is a dimensionless density gradient

$$q(n, \nabla n) = \frac{|\nabla n|}{2k_s n}, \quad (\text{S8})$$

where $k_s = 2(3n/\pi)^{1/6}$. In notation of Ref.², the PBE H function is

$$H(\varepsilon_c^{\text{LDA}}, \zeta, q) = \gamma \phi^3 \times \ln \left\{ 1 + \frac{\beta_c}{\gamma} q^2 \left[\frac{1 + A_{\text{PBE}} q^2}{1 + A_{\text{PBE}} q^2 + A_{\text{PBE}}^2 q^4} \right] \right\} \quad (\text{S9})$$

$$A_{\text{PBE}} = \frac{\beta_c}{\gamma} [\exp \{-\varepsilon_c^{\text{LDA}}/(\gamma \phi^3)\} - 1]^{-1} \quad (\text{S10})$$

$$\phi(\zeta) = \frac{1}{2} [(1 + \zeta)^{2/3} + (1 - \zeta)^{2/3}] \quad (\text{S11})$$

with $\gamma = (1 - \ln 2)/\pi^2$.

II. KDT16 EXCHANGE-CORRELATION FREE-ENERGY

Structure of the KDT16 exchange-correlation free-energy is similar to the PBE density functional, except that the KDT16 depends on variables and functions with explicit temperature dependence (via reduced temperature $t = T/T_F \equiv 2k_B T/[3\pi^2 n]^{2/3}$)

$$\mathcal{F}_{xc}^{\text{KDT16}}[n, T] = \mathcal{F}_x^{\text{KDT16}}[n, T] + \mathcal{F}_c^{\text{KDT16}}[n, T]. \quad (\text{S12})$$

A. Exchange free-energy

The KDT16 exchange free-energy density functional

$$\mathcal{F}_x^{\text{KDT16}}[n, T] = \int n f_x^{\text{LDA}}(n, T) F_x^{\text{KDT16}}(s_{2x}) d\mathbf{r}, \quad (\text{S13})$$

depends on the LDA free-energy per particle which has the factorized form

$$f_x^{\text{LDA}}(n, T) = \varepsilon_x^{\text{LDA}}(n) \tilde{A}_x(t), \quad (\text{S14})$$

with the t -dependent function $\tilde{A}_x(t)$ given by the explicit analytic fit⁴ in terms of variable $y = 2/3t^{3/2}$ (with $u = y^{2/3}$, and $v = y^{4/3}$)

$$\tilde{A}_x(y) = \frac{a_{\ln} y^4 \ln(y) + a_{2.5} u^{5/2} + \sum_{i=1}^8 a_i u^i}{1 + \sum_{i=1}^4 b_i v^i}, \quad (\text{S15})$$

and coefficient values tabulated in Table S1. The KDT16 exchange enhancement factor is a simple function

$$F_x(s_{2x}) = 1 + \frac{\nu_x s_{2x}}{1 + \alpha |s_{2x}|}, \quad (\text{S16})$$

TABLE S1: Coefficients in fit to $\tilde{A}_x(y)$ Eq. (S15).

coefficient	value
a_{ln}	-0.0475410604245741
$a_{2.5}$	-0.1065378473507800
a_1	0.5823869764908659
a_2	-0.0068339509356661
a_3	11.5469239288490009
a_4	-0.8465428870889800
a_5	-0.1212525366470300
a_6	1.9902818786101000
a_7	0.0000000000000000
a_8	0.0744389046707120
b_1	19.9256144707979992
b_2	5.1663994545590004
b_3	2.0463164858237000
b_4	0.0744389046707120

TABLE S2: Coefficients in fit to $\tilde{B}_x(y)$.

coefficient	value
a_2	-3.4341427276599950
a_3	-0.9066069544311700
a_4	2.2386316137237001
a_5	2.4232553178542000
a_6	-0.1339278564306200
a_7	0.4392739633708200
a_8	-0.0497109675177910
a_9	0.0000000000000000
a_{10}	0.0028609701106953
b_1	0.7098198258073800
b_2	4.6311326377185997
b_3	-2.9243190977647000
b_4	6.1688157841895004
b_5	-1.3435764191535999
b_6	0.1576046383295400
b_7	0.4365792821186800
b_8	-0.0620444574606262
b_9	0.0000000000000000
b_{10}	0.0028609701106953

of the exchange free-energy reduced density gradient

$$s_{2x}(n, \nabla n, T) \equiv s^2(n, \nabla n) \frac{\tilde{B}_x(t)}{\tilde{A}_x(t)}, \quad (\text{S17})$$

and two parameters consistent with the PBE ground-state exchange, $\nu_x = \mu = 0.21951$ and $\alpha = \mu/\kappa = 0.27302$. The accurate fit for $\tilde{B}_x(t)$ as an explicit function of y (or a function of t after a variable change) is given in Ref.⁴ as following

$$\tilde{B}_x(y) = \frac{\sum_{i=2}^{10} a_i u^i}{1 + \sum_{i=1}^{10} b_i u^i}, \quad (\text{S18})$$

and coefficient values tabulated in Table S2.

TABLE S3: Parameters for the $\tilde{B}_c(r_s, t)$ fit, Eq. (S22).

i	a_i	b_i	c_i
1	0.30047773E+03	-0.11166044E+03	0.32175261E+02
2	-0.38706401E+03	-0.45327975E+02	0.61853048E+02
3	0.25112237E+04	-0.14507109E+04	0.33585054E+03
4	0.52243427E+03	-0.30665095E+02	0.12874241E+03
	d_i	e_i	f_i
1	0.11077393E+03	0.12854960E+01	0.41006057E-02
2	0.32355494E+03	0.13482659E+02	0.18933118E-01
3	0.45509212E+03	0.23416018E+02	0.24295413E-04
4	0.10884352E+04	0.24480831E+02	0.18369776E-07
5	0.36112605E+00	0.32161372E-08	0.69274681E-10

B. Correlation free-energy

The KDT16 correlation free-energy density functional is defined in terms of the correlation free-energy per particle

$$\mathcal{F}_c^{\text{KDT16}}[n, T] = \int n f_c^{\text{KDT16}}(n, \nabla n, T) d\mathbf{r}, \quad (\text{S19})$$

which takes the PBE form with explicit T -dependence introduced via reduced density gradient for correlation defined on the base of the finite- T gradient expansion for correlation

$$q_c(n, \nabla n, T) = q(n, \nabla n) \sqrt{\tilde{B}_c(n, t)}, \quad (\text{S20})$$

$$f_c^{\text{KDT16}}(n, \nabla n, T) = f_c^{\text{LDA}}(n, T) + H\left(f_c^{\text{LDA}}, \zeta = 0, q_c\right), \quad (\text{S21})$$

where f_c^{LDA} is the LDA correlation free-energy per particle given by the corrected Karasiev-Sjostrom-Dufty-Trickey (corrKSDT) parameterization^{2,5} ($f_c^{\text{LDA}} \equiv f_c^{\text{corrKSDT}, \zeta=0}$), ζ is the spin polarization fraction, and H is as defined by in Eq. (S9). Density and temperature dependent function \tilde{B}_c in Eq. (S20) is given by a Padé approximant of order [4,5] with respect to the variable $u = t^{13/4}$ and with density dependent coefficients (via $r_s = (3/4\pi n)^{1/3}$ variable

$$\tilde{B}_c(r_s, t) = \frac{1 + \sum_{i=1}^4 (a_i + b_i r_s^{1/2} + c_i r_s) u^i}{1 + \sum_{i=1}^5 (d_i + e_i r_s^{3/2} + f_i r_s^3) u^i}. \quad (\text{S22})$$

The final set of parameters is given in Table S3.

The corrKSDT LDA functional (see^{2,5}) provides an analytical expression for the XC free-energy per particle f_{xc}^{corrKSDT} . The corresponding correlation free-energy per particle f_c^{corrKSDT} is calculated as

$$f_c^{\text{corrKSDT}}(n, T) = f_{xc}^{\text{corrKSDT}}(n, T) - f_x^{\text{LDA}}(n, T), \quad (\text{S23})$$

where $f_x^{\text{LDA}} = \varepsilon_x^{\text{LDA}} \tilde{A}_x(t)$ is the LDA exchange free-energy per particle, Eq. (S14).

TABLE S4: Parameters for the corrected KSDT XC free-energy functional (corrKSDT), defined by Eqs. (9)-(14) in Ref.⁵ for the unpolarized ($\zeta = 0$) case. $\lambda = (4/9\pi)^{1/3}$.

b_1	0.342554
b_2	9.141315
b_3	0.448483
b_4	18.553096
b_5	$\sqrt{3/2} \lambda^{-1} b_3 = 1.054151$
c_1	0.875130
c_2	-0.256320
c_4	0.953988
d_1	0.725917
d_2	2.237347
d_3	0.280748
d_4	4.185911
d_5	0.692183
e_1	0.255415
e_2	0.931933
e_3	0.115398
e_4	17.234117
e_5	0.451437

The spin-unpolarized f_{xc}^{corrKSDT} is given by the following Padé approximant with t -dependent coefficients

$$f_{xc}^{\zeta=0}(r_s, t) = -\frac{1}{r_s} \frac{a(t) + b_\zeta(t)r_s^{1/2} + c_\zeta(t)r_s}{1 + d_\zeta(t)r_s^{1/2} + e_\zeta(t)r_s}, \quad (\text{S24})$$

The functions $a(t)$, $b_\zeta(t) - e_\zeta(t)$, in turn, are Padé approximants in t

$$a(t) = 0.610887 \tanh\left(\frac{1}{t}\right) \times \frac{0.75 + 3.04363t^2 - 0.09227t^3 + 1.7035t^4}{1 + 8.31051t^2 + 5.1105t^4} \quad (\text{S25})$$

$$b(t) = \tanh\left(\frac{1}{\sqrt{t}}\right) \frac{b_1 + b_2t^2 + b_3t^4}{1 + b_4t^2 + b_5t^4} \quad (\text{S26})$$

$$c(t) = \left[c_1 + c_2 \exp\left(-\frac{c_3}{t}\right) \right] e(t) \quad (\text{S27})$$

$$d(t) = \tanh\left(\frac{1}{\sqrt{t}}\right) \frac{d_1 + d_2t^2 + d_3t^4}{1 + d_4t^2 + d_5t^4} \quad (\text{S28})$$

$$e(t) = \tanh\left(\frac{1}{t}\right) \frac{e_1 + e_2t^2 + e_3t^4}{1 + e_4t^2 + e_5t^4}. \quad (\text{S29})$$

Table S4 provides parameters in Eqs. (S26)-(S29) for the corrected functional, corrKSDT.

III. STRONGLY CONSTRAINED AND APPROPRIATELY NORMED WITH LAPLACIAN DEPENDENCE

The full set of equations for the strongly constrained and appropriately normed with Laplacian dependence (SCAN-L) ground-state exchange-correlation energy density functional is given below. The SCAN-L

exchange-correlation is a sum of exchange and correlation

$$E_{xc}^{\text{SCAN-L}}[n] = E_x^{\text{SCAN-L}}[n] + E_c^{\text{SCAN-L}}[n], \quad (\text{S30})$$

Exchange has a meta-GGA semi-local form⁶

$$E_x^{\text{SCAN-L}}[n] = \int n(\mathbf{r}) \varepsilon_x^{\text{LDA}}(n) F_x^{\text{SCAN-L}}(s, \alpha) d\mathbf{r}, \quad (\text{S31})$$

The SCAN-L exchange enhancement factor is given by

$$F_x^{\text{SCAN-L}}(s, \alpha) = \left[h_x^1(s, \alpha) + f_x(\alpha) \{ 1.174 - h_x^1(s, \alpha) \} \right] g_x(s), \quad (\text{S32})$$

where $\theta(y)$ is a step function of y , α is the Laplacian-dependent kinetic-energy-based region detector defined below in Eq. (S47) and

$$g_x(s) = 1 - e^{-a_1/\sqrt{s}} \quad (\text{S33})$$

$$f_x(\alpha) = e^{-c_{1x}\alpha/(1-\alpha)}\theta(1-\alpha) - d_x e^{c_{2x}/(1-\alpha)}\theta(\alpha-1) \quad (\text{S34})$$

$$h_x^1(s, \alpha) = 1 + \frac{k_1 x}{k_1 + x} \quad (\text{S35})$$

$$x = \mu_{\text{GE}} s^2 \left[1 + \frac{b_4 s^2}{\mu_{\text{GE}}} e^{-b_4 s^2/\mu_{\text{GE}}} \right] + [b_1 s^2 + b_2(1-\alpha)e^{-b_3(1-\alpha)^2}]^2. \quad (\text{S36})$$

The constants in Eqs. (S33)-(S36) take the following values

$$a_1 = 4.9479 \quad (\text{S37})$$

$$\mu_{\text{GE}} = \frac{10}{81} \quad (\text{S38})$$

$$b_2 = \sqrt{\frac{5913}{405000}} \quad (\text{S39})$$

$$b_1 = \frac{511}{13500} \frac{1}{2b_2} \quad (\text{S40})$$

$$b_3 = 0.5 \quad (\text{S41})$$

$$b_4 = \frac{\mu_{\text{GE}}^2}{k_1} - \frac{1606}{18225} - b_1^2 \quad (\text{S42})$$

$$c_{1x} = 0.667 \quad (\text{S43})$$

$$c_{2x} = 0.8 \quad (\text{S44})$$

$$d_{1x} = 1.24 \quad (\text{S45})$$

$$k_1 = 0.065. \quad (\text{S46})$$

The Laplacian-dependent kinetic-energy-based region detector is

$$\alpha(n, \nabla n, \nabla^2 n) \equiv (t_s^{\text{PCopt}} - t_W)/t_{\text{TF}}, \quad (\text{S47})$$

where the orbital-free Thomas-Fermi (TF) and von Weizsäcker (VW) are

$$t_{\text{TF}}(n) = c_{\text{TF}} n^{5/3}(\mathbf{r}), \quad (\text{S48})$$

$$c_{\text{TF}} = \frac{3}{10} (3\pi^2)^{2/3}, \quad (\text{S49})$$

$$t_W(n, \nabla n) = \frac{5}{3} t_{\text{TF}} s^2. \quad (\text{S50})$$

The re-optimized Perdew-Constantin PCopt kinetic energy density, t_s^{PCopt} , is defined by the following set of equations

$$F_t^{(2)} = \frac{5}{27}s^2 + \frac{20}{9}p, \quad (\text{S51})$$

$$F_t^{(4)} = \frac{8}{81}p^2 - \frac{1}{9}s^2p + \frac{8}{243}s^4, \quad (\text{S52})$$

$$F_t^{\text{W}} = \frac{5}{3}s^2, \quad (\text{S53})$$

$$F_t^{\text{MGE4}} = \frac{1 + F_t^{(2)} + F_t^{(4)}}{\sqrt{1 + [F_t^{(4)}/(1 + F_t^{\text{W}})]^2}}, \quad (\text{S54})$$

$$z^{\text{PC}} = F_t^{\text{MGE4}} - F_t^{\text{W}}, \quad (\text{S55})$$

$$F_t^{\text{PCopt}} = F_t^{\text{W}} + z^{\text{PC}}\theta_{\text{PC}}(z^{\text{PC}}), \quad (\text{S56})$$

$$t_s^{\text{PCopt}} = t_{\text{TF}}F_t^{\text{PCopt}}. \quad (\text{S57})$$

The PCopt interpolation function in Eq. (S56) is

$$\theta_{\text{PC}}(z) = \begin{cases} 0, & z \leq 0, \\ \left[\frac{1+e^{a/(a-z)}}{e^{a/z}+e^{a/(a-z)}} \right]^b, & 0 < z < a, \\ 1, & z \geq a. \end{cases} \quad (\text{S58})$$

with the re-optimized parameter values $a = 0.5389$ and $b = 3$.

The SCAN-L correlation has the form

$$E_c^{\text{SCAN-L}}[n] = \int n(\mathbf{r}) \left[\varepsilon_c^1 + f_c(\alpha)(\varepsilon_c^0 - \varepsilon_c^1) \right] d\mathbf{r}, \quad (\text{S59})$$

with

$$f_c(\alpha) = e^{-c_{1c}\alpha/(1-\alpha)}\theta(1-\alpha) - d_c e^{c_{2c}/(1-\alpha)\theta(\alpha-1)}, \quad (\text{S60})$$

where $c_{1c} = 0.64$, $d_c = 0.7$, and $c_{2c} = 1.5$. Two revised PBE correlation energies per particle, ε_c^0 and ε_c^1 , valid for $\alpha = 0$ and $\alpha = 1$ have definitions similar to Eqs. (S7)

$$\varepsilon_c^{0/1}(n, \nabla n) = \varepsilon_c^{\text{LDA},0/1}(n) + H_{0/1}(\varepsilon_c^{\text{LDA},0/1}, q), \quad (\text{S61})$$

with revised forms of $\varepsilon_c^{\text{LDA},0/1}$ and $H_{0/1}$ functions Eq. (S9) (more details can be found in Ref.^{7,10}, see also the explicit Eqs. (S24)-(S42) in Supporting Information for Ref.¹⁰).

IV. FINITE- T CONSTRAINTS SATISFIED BY THE T-SCAN-L EXCHANGE AND CORRELATION

In this Section we list some of constraints satisfied by the T-SCAN-L exchange and correlation at finite- T inherited correctly from the KDT16 XC free-energy density functional².

(i) Ground-state SCAN-L and PBE XC functionals, in the constant density limit, recover the zero-temperature homogeneous electron gas (HEG) XC limit; the finite- T KDT16 recovers correctly the finite- T HEG limit, such that eventually the SCAN-L and PBE zero- T HEG terms in Eqs. (2)-(3) cancel out, and the T-SCAN-L recovers correctly the HEG limit at all T .

(ii) The T-SCAN-L XC functional in the small- s limit recovers the T dependence of the finite- T second-order gradient expansion (for both exchange and correlation terms), i.e. it reproduces the slowly varying regime correctly up to second-order terms for all T .

(iii) The T-SCAN-L XC reduces to the finite- T LDA XC free-energy in the high- T asymptotic limit for any density with finite reduced density gradient value. This constraint is a consequence of the finite- T gradient expansion and is satisfied approximately up to the remainder of the cancellation between the ground-state SCAN-L and PBE gradient expansion terms.

(iv) The T-SCAN-L exchange satisfies one of the known exact scaling relation^{8,9} $\mathcal{F}_x^{\text{T-SCAN-L}}[n_\lambda, T] = \lambda \mathcal{F}_x^{\text{T-SCAN-L}}[n, T/\lambda^2]$, with $n_\lambda(\mathbf{r}) = \lambda^3 n(\lambda\mathbf{r})$, due to the T-SCAN-L temperature dependences are defined on the base of the physically motivated finite- T gradient expansion.

V. ACKNOWLEDGMENTS

This report was prepared as an account of work sponsored by an agency of the U.S. Government. Neither the U.S. Government nor any agency thereof, nor any of their employees, makes any warranty, express or implied, or assumes any legal liability or responsibility for the accuracy, completeness, or usefulness of any information, apparatus, product, or process disclosed, or represents that its use would not infringe privately owned rights. Reference herein to any specific commercial product, process, or service by trade name, trademark, manufacturer, or otherwise does not necessarily constitute or imply its endorsement, recommendation, or favoring by the U.S. Government or any agency thereof. The views and opinions of authors expressed herein do not necessarily state or reflect those of the U.S. Government or any agency thereof.

This material is based upon work supported by the Department of Energy National Nuclear Security Administration under Award Number DE-NA0003856 and US National Science Foundation PHY Grant No. 1802964. This research used resources of the National Energy Research Scientific Computing Center, a DOE Office of Science User Facility supported by the Office of Science of the U.S. Department of Energy under Contract No. DE-AC02-05CH11231.

* Corresponding Author: vkarsev@le.rochester.edu

- ¹ J.P. Perdew, K. Burke, and M. Ernzerhof, Phys. Rev. Lett. **77**, 3865 (1996); erratum *ibid.* **78**, 1396 (1997).
- ² V.V. Karasiev, J. Dufty, and S.B. Trickey, “Non-empirical Semi-local Free-Energy Density Functional for Matter Under Extreme Conditions”, Phys. Rev. Lett. **120**, 076401(1-7) (2018).
- ³ J.P. Perdew, and Y. Wang, Phys. Rev. B **45**, 13244 (1992).
- ⁴ V.V. Karasiev, D. Chakraborty, and S.B. Trickey, Comput. Phys. Commun. **192**, 114 (2015).
- ⁵ V.V. Karasiev, T. Sjostrom, J. Dufty, and S.B. Trickey, Phys. Rev. Lett. **112**, 076403 (2014).
- ⁶ D. Mejia-Rodriguez, and S.B. Trickey, “Deorbitalization Strategies for Meta-Generalized-Gradient-Approximation

Exchange-Correlation Functionals” Phys. Rev. A **96**, 052512(1-10) (2017).

- ⁷ J. Sun, A. Ruzsinszky, and J.P. Perdew, “Strongly Constrained and Appropriately Normed Semilocal Density Functional”, Phys. Rev. Lett. **115**, 036402(1-6) (2015).
- ⁸ S. Pittalis, C.R. Proetto, A. Floris, A. Sanna, C. Bersier, K. Burke, and E.K.U. Gross, Phys. Rev. Lett. **107**, 163001 (2011).
- ⁹ J.W. Dufty and S.B. Trickey, Mol. Phys. **114**, 988 (2016).
- ¹⁰ J.W. Furness, A.D. Kaplan, J. Ning, J.P. Perdew, and J. Sun, “Accurate and Numerically Efficient r²SCAN Meta-Generalized Gradient Approximation”, J. Phys. Chem. Lett. **11**, 8208-8215 (2020).